International Journal of Advances in Engineering and Management (IJAEM)
Volume 7, Issue 07 July 2025, pp: 500-514 www.ijaem.net ISSN: 2395-5252

Effect of Shape Factor on MHD Squeezing Flow between Parallel Disks Using Homotopy Perturbation Method (HPM)

[1]SAMUEL,P.O.,[2]RAHEEM,T.L.,[3*]ABASS,F.A.

[1,2]*Department of Mathematics, Lagos State University of Education*

[3*]*Department of Mathematics, Lagos State University, Ojo,Nigeria.*

Date of Submission: 05-07-2025 Date of Acceptance: 15-07-2025

ABSTRACT: This study investigates the influence of nanoparticle shape factors on the magnetohydrodynamic (MHD) squeezing flow and heat transfer characteristics of nanofluids between two parallel disks. The research employs the Homotopy Perturbation Method (HPM) to solve the coupled nonlinear ordinary differential equations governing the flow and thermal behavior. The nanofluid is modeled using the Hamilton-Crosser thermal conductivity model, which accounts for the shape factor (m) of nanoparticles, with specific focus on Platelet, Cylinder, and Brick-shaped nanoparticles. Key dimensionless parameters such as the squeeze number (S), Hartmann number (M), nanoparticle volume fraction (ϕ), Eckert number (Ec), and Prandtl number (Pr) are analyzed to understand their effects on velocity and temperature profiles. Results demonstrate that nanoparticle geometry significantly impacts fluid dynamics and heat transfer. Platelet-shaped nanoparticles exhibit the most pronounced deviations in velocity and temperature profiles due to their higher surface area-to-volume ratio. Increasing the nanoparticle volume fraction enhances momentum and thermal transport, while stronger magnetic fields (higher M) decelerate the flow and augment temperature gradients. The squeeze number (S) and Eckert number (Ec) further influence the flow and thermal boundary layers, with higher values leading to steeper gradients near the disk surfaces. The study highlights the critical role of nanoparticle shape and external parameters in optimizing nanofluid performance for applications in electronics cooling, lubrication systems, and energy-efficient heat transfer devices.

KEYWORDS: MHD flow, Nanofluids, Squeezing flow, Homotopy Perturbation Method, Nanoparticle shape factor, Heat transfer.

I. INTRODUCTION

Nanofluids are defined as stable suspensions or colloidal dispersions of nanoparticles within a base fluid, and they represent a new class of heat transfer fluids [10]. These fluids incorporate small quantities of nanoparticles that remain uniformly dispersed in the base medium. The typical size of these suspended nanoparticles is below 100 nanometers (nm). This novel concept was first introduced by [10], who coined the term “nanofluids.” Traditional base fluids generally exhibit poor thermal conductivity; therefore, efforts have been made to enhance their thermal performance. As noted by [21], engineers and scientists have contributed significantly to overcoming this limitation by dispersing micro- or millimeter-sized particles into liquids to improve their heat transfer characteristics. Nanofluids offer extensive applications across various fields, including electronics, power generation, air conditioning, and transportation.

[21] initially explored the idea of incorporating fine solid particles into fluids referred to as base fluids to increase their thermal conductivity. At that time, he used micrometer and millimeter sized particles for this purpose. Since then, numerous models have been proposed to describe the effective thermal conductivity of nanofluids; one such example is the Hamilton and Crosser model, which accounts for the influence of nanoparticle shape [8]. Within this model, a key parameter m, known as the shape factor, plays an important role. When $m = 3$, the Hamilton and

International Journal of Advances in Engineering and Management (IJAEM)
Volume 7, Issue 07 July 2025, pp: 500-514 www.ijaem.net ISSN: 2395-5252

Crosser model simplifies to the Maxwell-Garnett model, which applies specifically to spherical particles.

Given the wide-ranging applications of nanofluids, researchers have increasingly focused on studying their behavior under various flow conditions. Recently, [12] investigated the fully developed squeezing flow of nanofluids between two parallel disks, considering three types of nanoparticles: magnetite (Fe_3O_4), manganese-zinc ferrite ($Mn-ZnFe_2O_4$), and cobalt ferrite ($CoFe_2O_4$). The foundational work on squeeze flow in lubrication systems was first studied by Stefan [33]. [24] further examined the squeezing flow between parallel plates, highlighting its physical characteristics. Additionally, [30] analyzed nanofluid flows in different geometries. In another study, [17] evaluated the flow and heat transfer characteristics of copper-water nanofluids using the Hamilton and Crosser model to estimate effective thermal conductivity.

To solve the governing equations of such flow problems, researchers often employ analytical methods such as Adomian's Decomposition Method (ADM) [32] and the Variation of Parameters Method (VPM) [23]. In 2015, [22] studied magnetohydrodynamic (MHD) flow and heat transfer of nanofluids in convergent/divergent channels, assuming that the channel walls were capable of stretching and shrinking. They applied the Maxwell-Garnett model for thermal conductivity and solved the resulting system of dimensionless ordinary differential equations using iterative techniques. For further analytical solutions of similar flow problems, see [22, 15, 16, 17, 7, 18].

In 2016,[28] presented analytical solutions for the MHD squeezing flow of nanofluids in rotating channels with a lower stretching surface using the Variational Iteration Method. They also conducted a thermohydrodynamic analysis of lubricant flows containing carbon-based nanoparticles [27]. Earlier, in 2015, [1] discussed how the geometry of nanoparticles affects thermal conductivity. Studies by [3] and [6] explored the impact of variable thermal conductivity and thermal radiation on flows over stretching surfaces. Numerical investigations into the magnetohydrodynamic transport of nanofluids over stretching sheets have also been reported in the literature. For additional studies on nanofluid flow in diverse contexts, refer to [5, 4, 31, 11, 29, 9, 2, 13].

Exact solutions for nonlinear coupled systems of differential equations are rare. While exact solutions may exist under specific conditions, they are generally difficult to obtain. As a result, researchers have shifted focus toward approximate analytical techniques and numerical methods. Several such methods have been proposed in the literature, including Adomian's Decomposition Method (ADM) [32], the Variation of Parameters Method (VPM) [23], and the Differential Transform Method (DTM), among others [31, 11, 29]. Numerical methods such as Runge-kutta Felberg method [25, 26]

II. MATHEMATICAL FORMULATION OF THE PROBLEM

Consider the axisymmetric and unsteady squeezing flow of an incompressible fluid between two parallel disks. The flow is an electrically conducting and the disks are apart at a distance $z = \pm H(1-\alpha t)^{\frac{1}{2}}$, where h is a function of t. The dimensions of α and t are inverse with each other. A magnetic field $\mathbf{B}_0$ of uniform strength is applied perpendicular to disks and this magnetic field is proportional to $\left(\frac{\mathbf{B}_0^2}{1-\alpha t}\right)^{\frac{1}{2}}$. The upper disk is capable to move toward or away with the velocity $\frac{dh}{dt}$ from the lower disks and lower disks are stationary and are situated at $z = 0$. Furthermore, the upper disks are at the height $z = h(t)$. The physical model is taken in cylindrical coordinates system (r, θ, z). As above it is mentioned that flow is axisymmetric $\left(\frac{\partial}{\partial \theta}(\cdot) = 0\right)$. Thus, the v component of the velocity vanishes and we have u and w components of the velocity along r and z directions, respectively. These are called radial and axial components of the velocity. The temperature at the lower disk is denoted by T_w, and at the upper disk is T_h (see Fig. 1). As a result under aforementioned assumptions,the governing equations for unsteady squeezing flow and heat transfer of viscous incompressible fluid can be written as follows [27]

International Journal of Advances in Engineering and Management (IJAEM)
Volume 7, Issue 07 July 2025, pp: 500-514 www.ijaem.net ISSN: 2395-5252

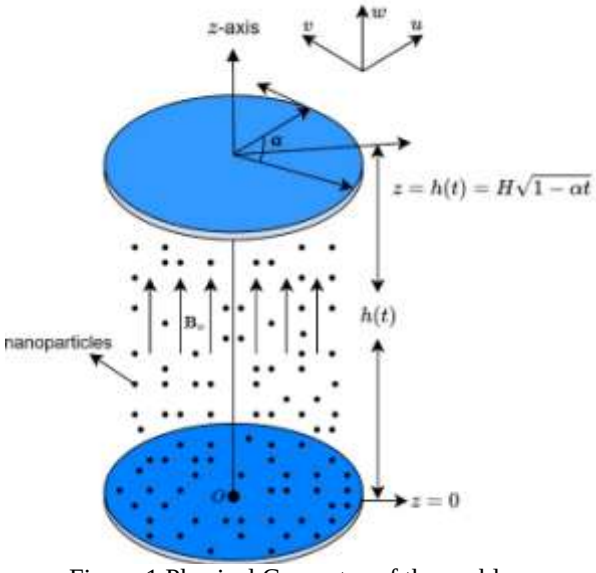

Figure 1 Physical Geometry of the problem

$$\frac{\partial u}{\partial r}+\frac{u}{r}+\frac{\partial w}{\partial z}=0 \quad \#(1)$$

$$\frac{\partial u}{\partial t}+u\frac{\partial u}{\partial r}+w\frac{\partial u}{\partial z}=\frac{1}{\rho_{nf}}\left(-\frac{\partial p}{\partial r}+\mu_{nf}\left(\frac{\partial^2 u}{\partial x^2}+\frac{\partial^2 u}{\partial y^2}\right)\right)-\frac{\sigma_{nf}\mathbf{B}_0^2}{\rho_{nf}}u, \quad \#(2)$$

$$\frac{\partial w}{\partial t}+u\frac{\partial w}{\partial r}+w\frac{\partial w}{\partial z}=\frac{1}{\rho_{nf}}\left(-\frac{\partial p}{\partial z}+\mu_{nf}\left(\frac{\partial^2 v}{\partial x^2}+\frac{\partial^2 v}{\partial y^2}\right)\right), \#(3)$$

$$\frac{\partial T}{\partial t}+u\frac{\partial T}{\partial r}+w\frac{\partial T}{\partial z}=\frac{1}{(\rho C_p)_{nf}}\left(k_{nf}\left(\frac{\partial^2 T}{\partial r^2}+\frac{1}{r}\frac{\partial T}{\partial r}+\frac{\partial^2 T}{\partial z^2}\right)+2\mu_{nf}\left(\left(\frac{\partial u}{\partial r}\right)^2+\left(\frac{u}{r}\right)^2+\left(\frac{\partial w}{\partial z}\right)^2+\frac{1}{2}\left(\frac{\partial u}{\partial z}+\frac{\partial w}{\partial r}\right)^2\right)\right), \quad \#(4)$$

The suilable boundary conditions for described flow model are [28,29] at $z = h(t)$

$$u = 0, w = \frac{dh}{dt}, u = T_w \ \#(5)$$

at $z = 0$

$$u = 0, w = -w_0, T = T_w \ \#(6)$$

In above equations, T and p are the temperature and pressure of the fluid, respectively. Moreover, $\sigma_{nf}, \rho_{nf}, \mu_{nf}$ represent the electrical conductivity, density, and viscosity of the nano-fluid,respectively [8].

$$\begin{aligned}\rho_{nf} &= (1-\phi)\rho_f+\phi\rho_s,\\ \mu_{nf} &= \frac{\mu_f}{(1-\phi)^{2.5}},\\ (\rho C_p)_n f &= (1-\phi)(\rho C_p)_f+\phi(\rho C_p)_s,\\ \sigma_{nf} &= \sigma_f\left[1+\frac{3\left\{\frac{\sigma_s}{\sigma_f}-1\right\}\phi}{\left\{\frac{\sigma_s}{\sigma_f}+2\right\}-\left\{\frac{\sigma_s}{\sigma_f}-1\right\}\phi}\right],\end{aligned} \quad \#(7)$$

The model contemplated, for the effective thermal conductivity of the nanofluid, is known as Hamilton Crosser's model [28]:

International Journal of Advances in Engineering and Management (IJAEM)
Volume 7, Issue 07 July 2025, pp: 500-514 www.ijaem.net ISSN: 2395-5252

$$k_{nf} = k_f \left[\frac{k_s + (m-1)k_f - (m-1)(k_f - k_s)\phi}{k_s + (m-1)k_f + (k_f - k_s)\phi} \right], \#(8)$$

where k_s, k_f, and m represent the conductivities of the nanoparticles, base fluid and nanoparticle shape factor. Also, ϕ is called the nanoparticle volume fraction. The shape factor m of nanoparticles is given by $\frac{3}{\psi}$ It is the sphericity. The sphericity is defined as the ratio of the surface area of the sphere and the surface area of the real particles with equal volumes. It is worth menuoning that the Hamilton Crosser's model becomes a Maxwell-Garnett's model, when the shape factor of nanoparticles is $m = 3$. The different shapes of nanoparticles with their sphericities are presented in Table 1.

The nondimensional parameters for the specific Now model are defined as follows:

$$\eta = \frac{z}{\left(H^2(1-\alpha t)\right)^{\frac{1}{2}}}, \quad u = \frac{\alpha x}{\left(2(1-\alpha t)\right)} f'(\eta), \quad w = \frac{\alpha H}{(1-\alpha t)} f(\eta), \quad \theta(\eta) = \frac{T - T_H}{T_w - T_H} \quad \#(9)$$

After entreating these nondimensional variables in Eqs.(2)-(4) and also differentiating the resulting equations w.r.t z and r, we have the following set of dimensionless coupled system of nonlinear ordinary differential equations

Table 1Sphericity and shape factor of different nanoparticle

Nanoparticles shapes	Aspect ratio	Sphericity	Shape factor
Platelet	1:1/8	0.52	5.7
Cylinder	1:8	0.62	4.9
Brick	1:1:1	0.81	3.7

$$f'''' - SK_1(1-\phi)^{2.5}(\eta f''' + 3f'' - 2ff''') - MB_1(1-\phi)^{2.5} f'' = 0 \quad (10)$$

$$\theta'' - \frac{PrSK_2}{K_1}(\eta\theta' - 2f\theta') + \frac{PrEc}{K_3(1-\phi)^{2.5}}(6\delta^2 f'^2 + f''^2) = 0 \quad (11)$$

where f and θ both depend on variable η. The nondimensional auxiliary conditions for Eqs. (10) and (11]) are as under the following:

$$f(0) = A, f'(0) = 0, f(1) = \frac{1}{2},$$
$$f'(1) = 0, \theta(0) = 1, \theta(1) = 0 \#(12)$$

In Eqs. (10]) and (11]), S denotes the Squeeze number, Pr is the Prandtl number, Ec is the Eckert number and Ha is the Hartmann number. These dimensionless parameters are as follows:

$$S = \frac{\alpha H^2}{2v_f}, Pr = \frac{v_f(\rho C_p)_f}{k_f}, Ec = \frac{1}{(T_w - T_H)}\left(\frac{\alpha x}{2(1-\alpha t)}\right)^2, \quad M = \frac{H^2 \boldsymbol{B}_0^2 \sigma_f}{\mu_f}, \delta = \frac{H^2}{x^2}(1-\alpha t) \quad \#(13)$$

The other ingrained parameters represented by $K_1; , K_2, K_3$ and $\boldsymbol{B}_1$, are as under the following:

$$K_1 = (1-\phi) + \phi\left\{\frac{\phi_s}{\phi_f}\right\},$$
$$K_2 = (1-\phi) + \phi\left\{\frac{(\rho C_p)_s}{(\rho C_p)_s}\right\},$$
$$K_3 = \left\{\frac{k_s + (m-1)k_f - (m-1)(k_f - k_s)\phi}{k_s + (m-1)k_f + (k_f - k_s)\phi}\right\}, \text{ and} \quad \#(13)$$
$$K_4 = \left\{\frac{(\sigma_s + 2\sigma_f) + 2(\sigma_s - 2\sigma_f)\phi}{(\sigma_s + 2\sigma_f) - (\sigma_s - 2\sigma_f)\phi}\right\}$$

International Journal of Advances in Engineering and Management (IJAEM)
Volume 7, Issue 07 July 2025, pp: 500-514 www.ijaem.net ISSN: 2395-5252

The mathematical expression for skin fraction coefficient and local rate of heat transfer in dimensional form is as follows:

$$C_{fr} = \frac{\mu_{nf}\left(\frac{\partial u}{\partial z}\right)_{z=h(t)}}{\rho_{nf}} \text{ and} Nu = -\frac{K_{nf}}{k_f}\frac{H\left(\frac{\partial u}{\partial z}\right)_{z=h(t)}}{(T_w - T_H)} \quad \#(15)$$

After some simplification, we have the following nondimensional form of skin fraction coefficient and local Nusselt number:

$$\begin{aligned}(1-\alpha t)^{\frac{3}{2}} R_{er} C_{fr} &= \frac{K_1}{(1-\phi)^{2.5}} F''(1), \\ \frac{(1-\alpha t)^{\frac{1}{2}}}{(T_w - T_H)} Nu &= -K_3 \beta'(1),\end{aligned} \quad \#(16)$$

where α and t are in reverse dimensions and $R_{er} = \frac{\alpha x v_f}{2H}$,

III. SOLUTION OF THE PROBLEM

In this section, we will apply the HPM to the system of nonlinear ordinary differential equation in (10)-(11) with the boundary condition (12). Using homotopy technique propose by [14] and , we can construct a homotopy $\mathcal{H}(\eta, p): \Omega \times [0,1] \to \mathbb{R}$ of a system (10)-(11) as follows

$$(1-p)f'''' + p(f'''' - SK_1(1-\phi)^{2.5}(\eta f''' + 3f'' - 2ff''') - MB_1(1-\phi)^{2.5} f'') = 0 \quad \#(17)$$

$$(1-p)\theta'' + p\left(\theta'' - \frac{PrSK_2}{K_1}(\eta\theta' - 2f\theta') + \frac{PrEc}{K_3(1-\phi)^{2.5}}(6\delta^2 f'^2 + f''^2)\right) = 0 \quad \#(18)$$

Solution of Eq. (10)-(11)is assumed in the form of a power series

$$\begin{aligned} f(\eta) &= f_0(\eta) + p^1 f_1(\eta) + p^2 f_2(\eta) + p^3 f_3(\eta) + p^4 f_4(\eta) + \cdots \\ \theta(\eta) &= \theta_0(\eta) + p^1\theta_1(\eta) + p^2\theta_2(\eta) + p^3\theta_3(\eta) + p^4\theta_4(\eta) + \cdots \end{aligned} \quad \#(19)$$

By substituting Eq. (19) into Eq. (17)-(18), we have

$$\begin{aligned} &(1-p)({f_0}^{(4)}(\eta) + p{f_1}^{(4)}(\eta) + p^2{f_2}^{(4)}(\eta) + p^3{f_3}^{(4)}(\eta) \\ &+p^4{f_4}^{(4)}(\eta) + p^5{f_5}^{(4)}(\eta) + p^6{f_6}^{(4)}(\eta)) \\ &+p(-M(1-\phi)^{2.5}B_1({f_0}''(\eta) + p{f_1}''(\eta) + p^2{f_2}''(\eta) + p^3{f_3}''(\eta) \\ &+p^4{f_4}''(\eta) + p^5{f_5}''(\eta) + p^6{f_6}''(\eta)) - S(1-\phi)^{2.5}k_1(3({f_0}''(\eta) \\ &+p{f_1}''(\eta) + p^2{f_2}''(\eta) + p^3{f_3}''(\eta) + p^4{f_4}''(\eta) + p^5{f_5}''(\eta) \\ &+p^6{f_6}''(\eta)) + \eta({f_0}^{(3)}(\eta) + \cdots \end{aligned} \quad \#(20)$$

$$\begin{aligned} &(1-p)({\theta_0}''(\eta) + p{\theta_1}''(\eta) + p^2{\theta_2}''(\eta) + p^3{\theta_3}''(\eta) + p^4{\theta_4}''(\eta) \\ &+p^5{\theta_5}''(\eta) + p^6{\theta_6}''(\eta)) + p(-\frac{PrSk_2}{k_3}(\eta({\theta_0}'(\eta) \\ &+p{\theta_1}'(\eta) + p^2{\theta_2}'(\eta) + p^3{\theta_3}'(\eta) + p^4{\theta_4}'(\eta) + p^5{\theta_5}'(\eta) \\ &+p^6{\theta_6}'(\eta)) - 2(f_0(\eta) + pf_1(\eta) + p^2f_2(\eta) + p^3f_3(\eta) \\ &+p^4f_4(\eta) + p^5f_5(\eta) + \cdots \end{aligned} \quad \#(21)$$

Collecting and equating coefficient of likes power of p to zero in Eq. (20) and (21), we have.

$$\begin{aligned} p^0&: {f_0}^{(4)}(\eta) = 0 \\ p^0&: {\theta_0}''(\eta) = 0 \end{aligned} \quad \#(22)$$

International Journal of Advances in Engineering and Management (IJAEM)
Volume 7, Issue 07 July 2025, pp: 500-514 www.ijaem.net ISSN: 2395-5252

$$p^1: -M(1-\phi)^{2.5}B_1 f_{0''}(\eta) - 3S(1-\phi)^{2.5}k_1 f_{0''}(\eta) - S\eta(1-\phi)^{2.5}k_1 f_0{}^{(3)}(\eta) + 2S(1-\phi)^{2.5}k_1 f_0(\eta) f_0{}^{(3)}(\eta) + f_1{}^{(4)}(\eta) = 0$$

$$p^1: \frac{6\mathrm{Ec}Pr\delta^2 f_{0'}(\eta)^2}{(1-\phi)^{2.5}k_3} - \frac{PrS\eta k_2\theta_{0'}(\eta)}{k_3} + \frac{2PrSk_2 f_0(\eta)\theta_{0'}(\eta)}{k_3} + \frac{\mathrm{Ec}Pr f_{0''}(\eta)^2}{(1-\phi)^{2.5}k_3} + \theta_{1''}(\eta) = 0 \quad \#(23)$$

$$p^2: -M(1-\phi)^{2.5}B_1 f_{1''}(\eta) - 3S(1-\phi)^{2.5}k_1 f_{1''}(\eta) + 2S(1-\phi)^{2.5}k_1 f_1(\eta) f_0{}^{(3)}(\eta) - S\eta(1-\phi)^{2.5}k_1 f_1{}^{(3)}(\eta) + 2S(1-\phi)^{2.5}k_1 f_0(\eta) f_1{}^{(3)}(\eta) + f_2{}^{(4)}(\eta) = 0$$

$$p^2: \frac{12\mathrm{Ec}Pr\delta^2 f_{0'}(\eta) f_{1'}(\eta)}{(1-\phi)^{2.5}k_3} + \frac{2PrSk_2 f_1(\eta)\theta_{0'}(\eta)}{k_3} - \frac{PrS\eta k_2\theta_{1'}(\eta)}{k_3} + \frac{2PrSk_2 f_0(\eta)\theta_{1'}(\eta)}{k_3} + \frac{2\mathrm{Ec}Pr f_{0''}(\eta) f_{1''}(\eta)}{(1-\phi)^{2.5}k_3} + \theta_{2''}(\eta) = 0 \quad \#(24)$$

We continue the process for $p^3, p^4, p^5, p^6, p^7, p^8, \cdots$. Then solving Eq. ([eq22])-([eq24]) with the following boundary conditions

$$f_n(0) = A, f_{n'}(0) = 0, f_n(1) = 0.5, f_{n'}(1) = 0, \quad \theta_n(0) = 1, \theta_n(1) = 0;\ n = 0,1,2,\cdots \quad \#(25)$$

Using Mathematica. The solution of ([eq10]) and ([eq11]) is obtain as follows,

$$f(\eta) = f_0(\eta) + f_1(\eta) + f_2(\eta) + f_3(\eta) + f_4(\eta) + \cdots \#(26)$$

$$\theta(\eta) = \theta_0(\eta) + \theta_1(\eta) + \theta_2(\eta) + \theta_3(\eta) + \theta_4(\eta) + \cdots \#(27)$$

IV. RESULT AND DISCUSSION

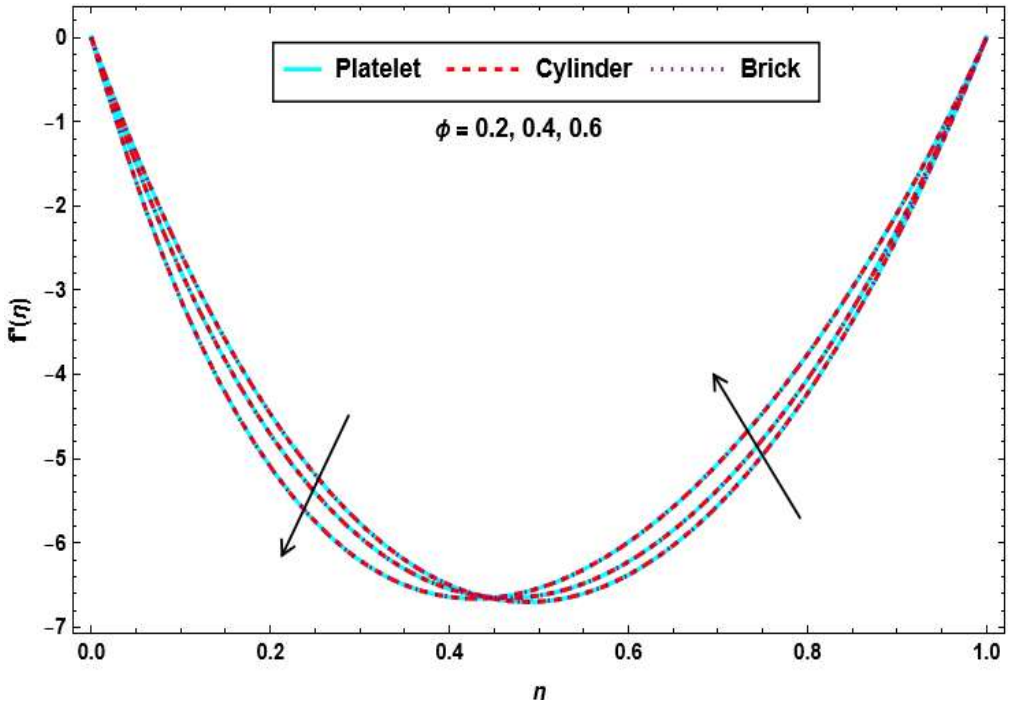

Figure 2 Effect of ϕ on velocity profile

International Journal of Advances in Engineering and Management (IJAEM)
Volume 7, Issue 07 July 2025, pp: 500-514 www.ijaem.net ISSN: 2395-5252

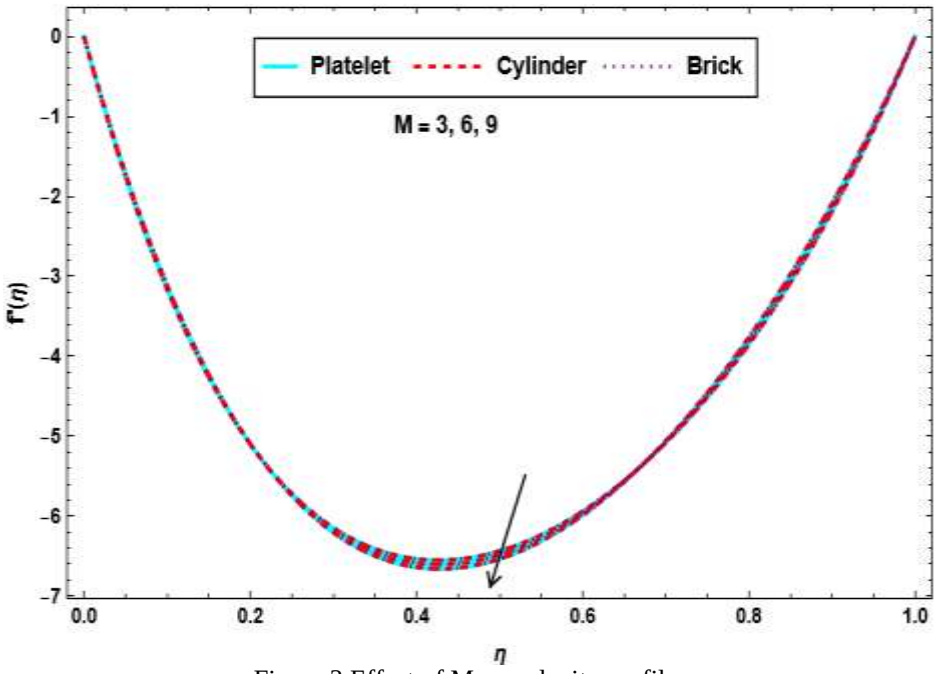

Figure 3 Effect of M on velocity profile

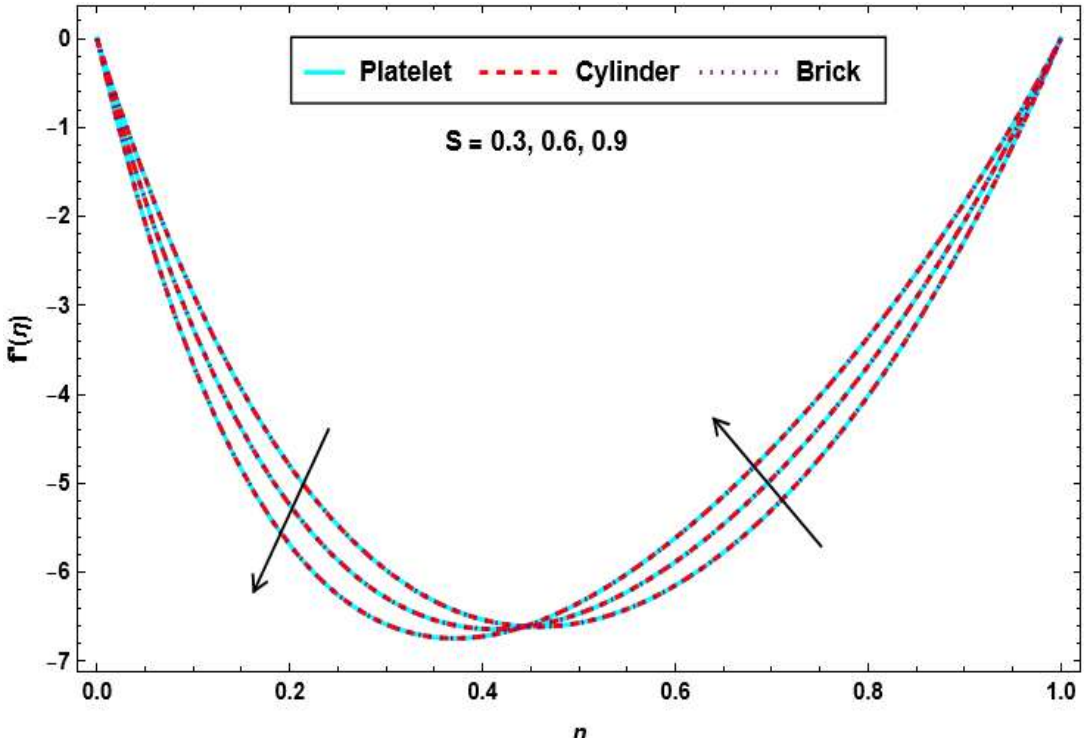

Figure 4 Effect of S on velocity profile

International Journal of Advances in Engineering and Management (IJAEM)
Volume 7, Issue 07 July 2025, pp: 500-514 www.ijaem.net ISSN: 2395-5252

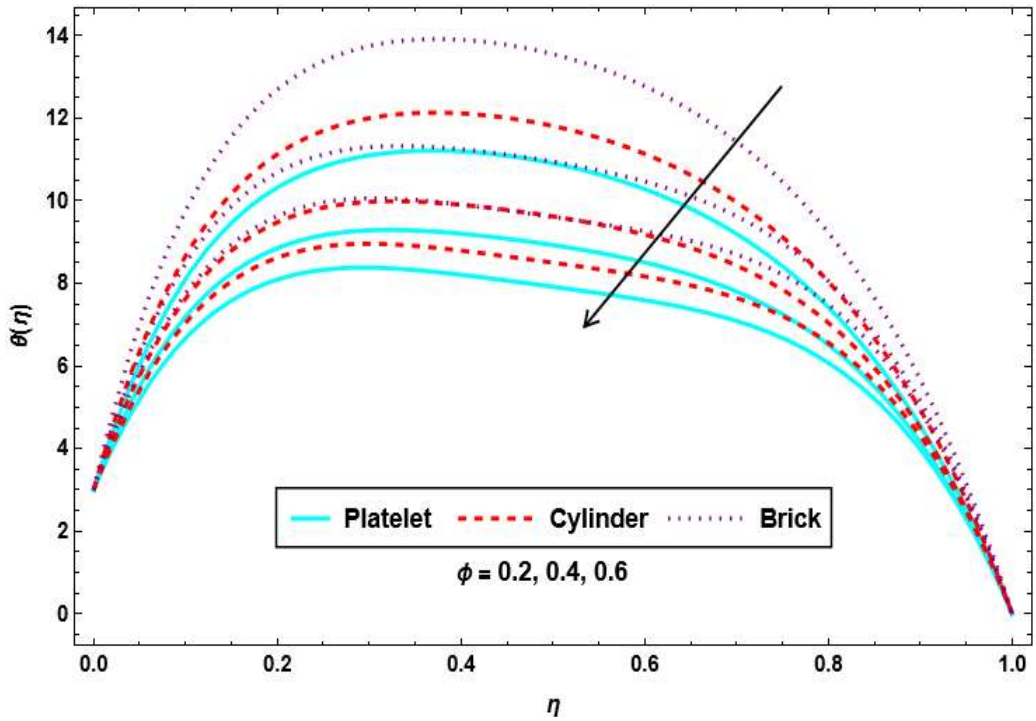

Figure 5 Effect of ϕ on temperature profile

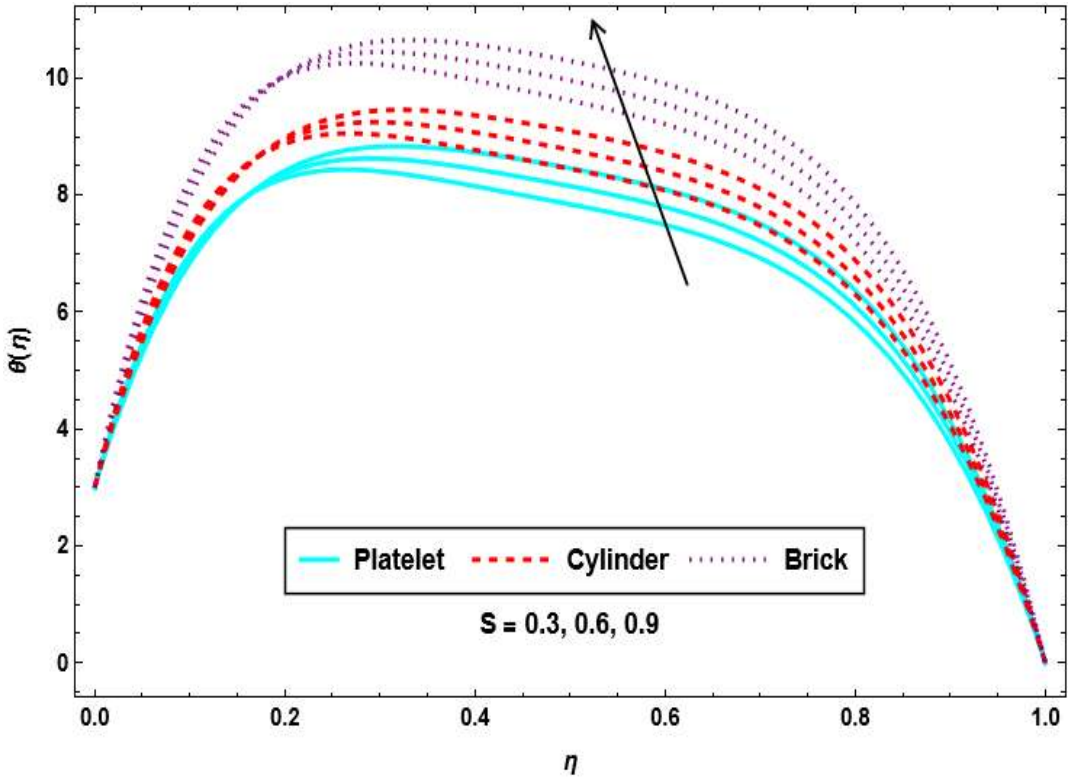

Figure 6 Effect of S on temperature on profile

International Journal of Advances in Engineering and Management (IJAEM)
Volume 7, Issue 07 July 2025, pp: 500-514 www.ijaem.net ISSN: 2395-5252

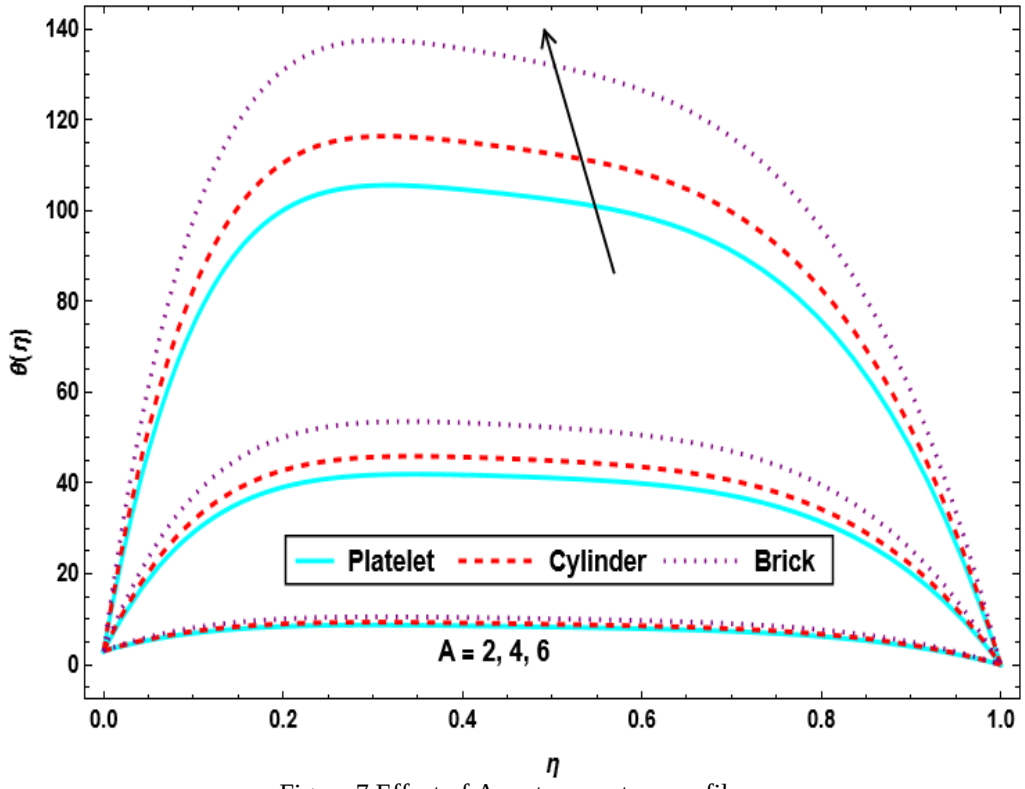

Figure 7 Effect of A on temperature profile

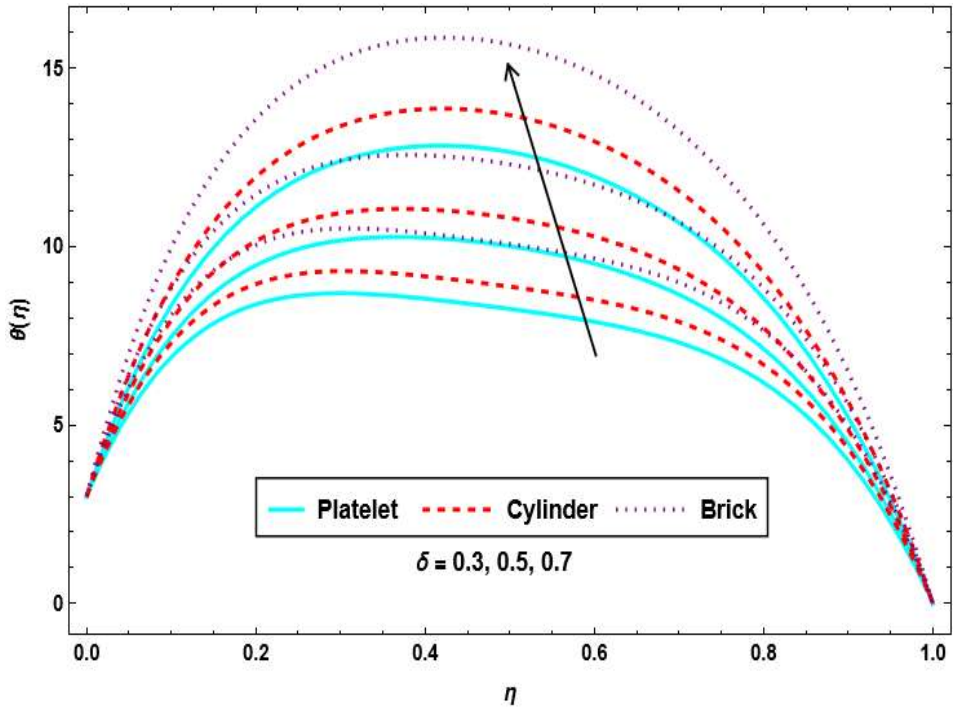

Figure 8 Effect of δ on temperature profile

International Journal of Advances in Engineering and Management (IJAEM)
Volume 7, Issue 07 July 2025, pp: 500-514 www.ijaem.net ISSN: 2395-5252

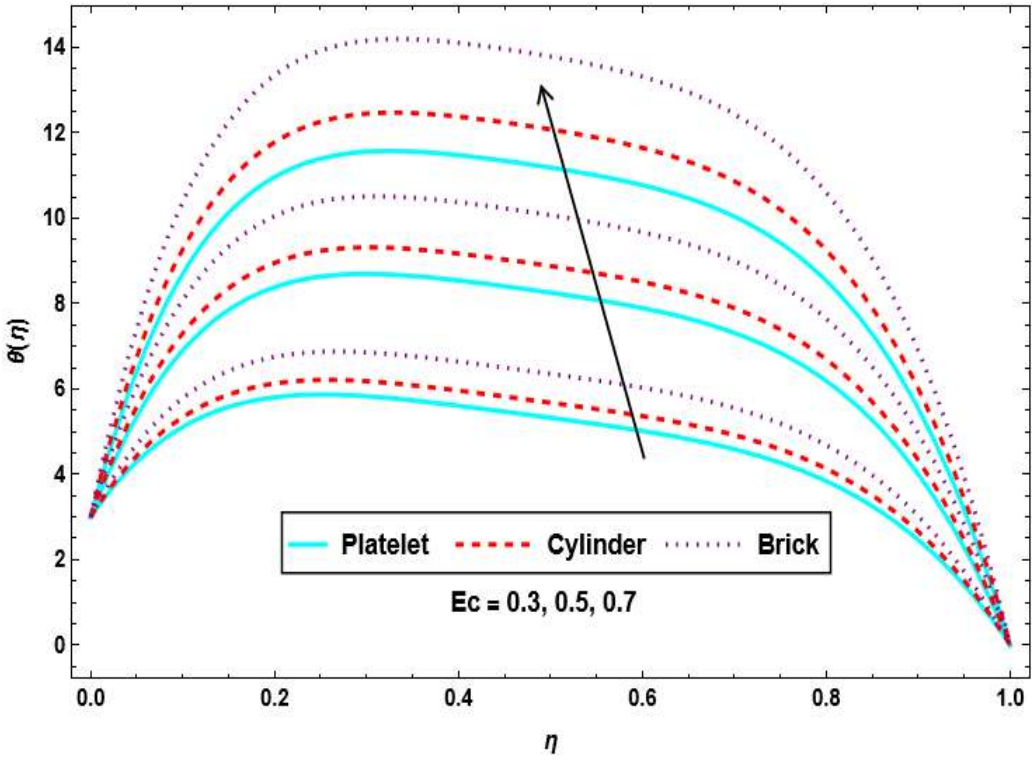

Figure 9 Effect of Ec on temperature profile

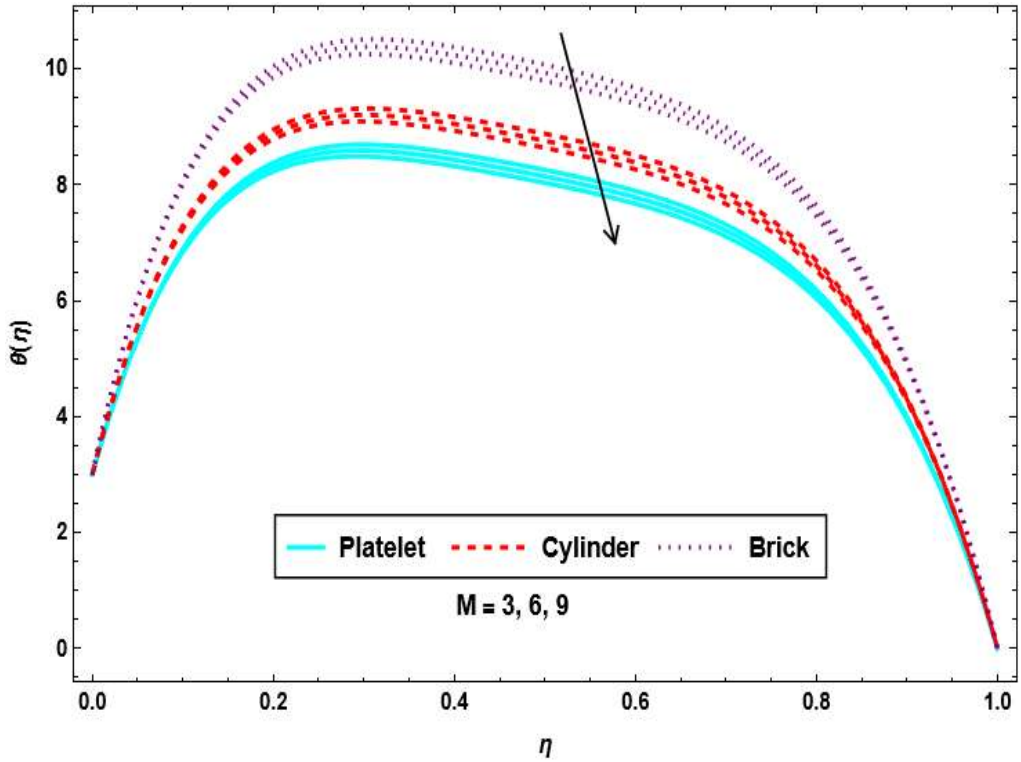

Figure 10 Effect of M on temperature profile

International Journal of Advances in Engineering and Management (IJAEM)
Volume 7, Issue 07 July 2025, pp: 500-514 www.ijaem.net ISSN: 2395-5252

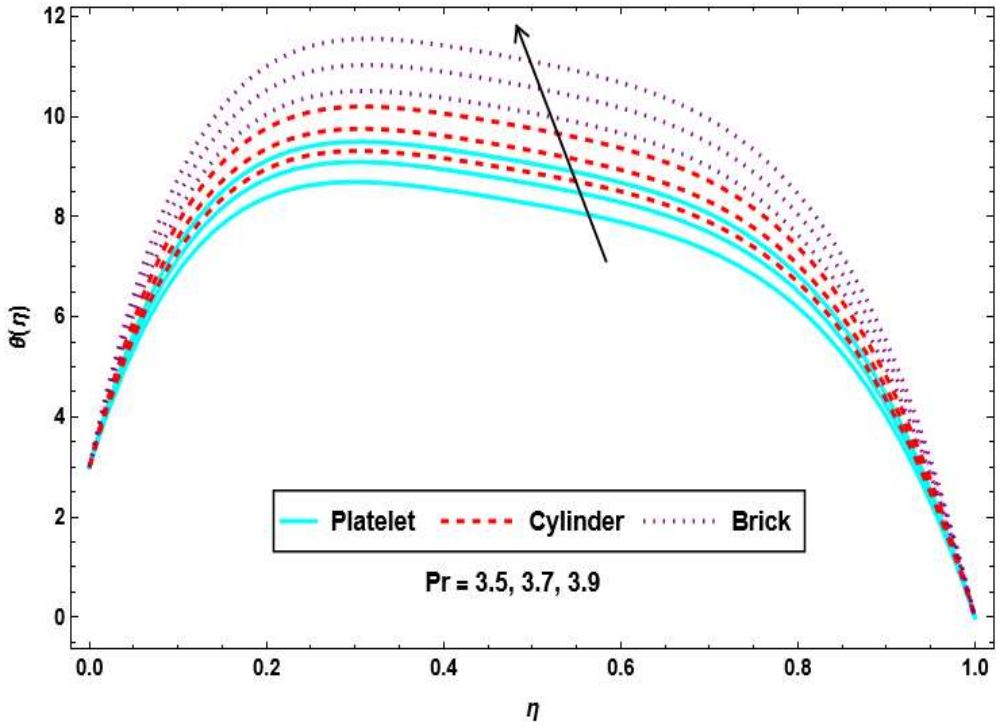

Figure 11 Effect of Pr on temperature profile

Figure 2 illustrates the velocity profiles of a magneto-nanofluid flow between two parallel disks for three different nanoparticle shapes Platelet, Cylinder, and Brick at varying nanoparticle volume fractions ($\phi = 0.2,\ 0.4$, and 0.6). The curves represent the dimensionless axial velocity component $f'(\eta)$ as a function of the similarity variable (η), highlighting how the shape factor of nanoparticles influences the fluid dynamics. As ϕ increases, the velocity profiles exhibit more pronounced curvature, indicating enhanced momentum transfer due to higher nanoparticle concentrations. The Platelet-shaped nanoparticles show the most significant deviation in velocity compared to Cylinder and Brick shapes, reflecting their larger surface area-to-volume ratio and stronger interaction with the base fluid. The convergence of all curves near $\eta = 1$ suggests boundary layer behavior, where the velocity approaches zero at the disk surfaces. This analysis underscores the critical role of nanoparticle geometry in controlling the flow characteristics of nanofluids under magnetic influence.

Figure 3 illustrates the velocity profiles $f'(\eta)$ of a magneto-nanofluid flow between two parallel disks for three different nanoparticle shapes Platelet, Cylinder, and Brick at varying Hartmann numbers ($M = 3,6,9$). The curves represent the dimensionless axial velocity gradient $f'(\eta)$ as a function of the similarity variable (η), highlighting how the magnetic field strength influences the fluid dynamics. As M increases, the velocity gradients become more pronounced, indicating stronger magnetic effects that decelerate the fluid near the boundaries. The Platelet-shaped nanoparticles (cyan line) exhibit the most significant deviation in velocity compared to Cylinder (red dashed line) and Brick (magenta dotted line) shapes, reflecting their larger surface area-to-volume ratio and stronger interaction with the base fluid. The convergence of all curves near $\eta = 1$ suggests boundary layer behavior, where the velocity approaches zero at the upper disk. This analysis underscores the critical role of both nanoparticle geometry and the magnetic field in controlling the flow characteristics of nanofluids under squeezed conditions.

Figure 4 illustrates the velocity profiles $f'(\eta)$ of a magneto-nanofluid flow between two parallel disks for three different nanoparticle shapes Platelet, Cylinder, and Brick at varying squeeze numbers ($S = 0.3,\ 0.6$, and 0.9). The curves represent the dimensionless axial velocity gradient $f'(\eta)$ as a function of the similarity variable η, highlighting how the squeeze number influences the fluid dynamics. As S increases, the velocity gradients become more pronounced, indicating stronger squeezing effects that decelerate the fluid near the boundaries. The Platelet-shaped nanoparticles (cyan line) exhibit the most

International Journal of Advances in Engineering and Management (IJAEM)
Volume 7, Issue 07 July 2025, pp: 500-514 www.ijaem.net ISSN: 2395-5252

significant deviation in velocity compared to Cylinder (red dashed line) and Brick (magenta dotted line) shapes, reflecting their larger surface area-to-volume ratio and stronger interaction with the base fluid. The convergence of all curves near $\eta = 1$ suggests boundary layer behavior, where the velocity approaches zero at the upper disk. This analysis underscores the critical role of both nanoparticle geometry and the squeeze number in controlling the flow characteristics of nanofluids under squeezed conditions.

Figure 5 illustrates the temperature profiles ($\theta(\eta)$) of a magneto-nanofluid flow between two parallel disks for three different nanoparticle shapes Platelet, Cylinder, and Brick at varying nanoparticle volume fractions ($\phi = 0.2$, 0.4, and 0.6). The curves represent the dimensionless temperature $\theta(\eta)$ as a function of the similarity variable (η), highlighting how the nanoparticle concentration influences the thermal behavior of the fluid. As ϕ increases, the temperature profiles exhibit more pronounced curvature, indicating enhanced heat transfer due to higher nanoparticle concentrations. The Platelet-shaped nanoparticles (cyan line) show the most significant deviation in temperature compared to Cylinder (red dashed line) and Brick (magenta dotted line) shapes, reflecting their larger surface area-to-volume ratio and stronger interaction with the base fluid. The convergence of all curves near $\eta = 1$ suggests boundary layer behavior, where the temperature approaches zero at the upper disk. This analysis underscores the critical role of nanoparticle geometry and concentration in controlling the thermal characteristics of nanofluids under squeezed conditions.

Figure 6 illustrates the temperature profiles $\theta(\eta)$ of a magneto-nanofluid flow between two parallel disks for three different nanoparticle shapes Platelet, Cylinder, and Brick at varying squeeze numbers ($S = 0.3$, 0.6, and 0.9). The curves represent the dimensionless temperature $\theta(\eta)$ as a function of the similarity variable η, highlighting how the squeeze number influences the thermal behavior of the fluid. As S increases, the temperature profiles exhibit more pronounced curvature, indicating enhanced heat transfer due to stronger squeezing effects. The Platelet-shaped nanoparticles (cyan line) show the most significant deviation in temperature compared to Cylinder (red dashed line) and Brick (magenta dotted line) shapes, reflecting their larger surface area-to-volume ratio and stronger interaction with the base fluid. The convergence of all curves near $\eta = 1$ suggests boundary layer behavior, where the temperature approaches zero at the upper disk. This analysis underscores the critical role of both nanoparticle geometry and the squeeze number in controlling the thermal characteristics of nanofluids under squeezed conditions.

Figure 7 illustrates the temperature profiles ($\theta(\eta)$) of a magneto-nanofluid flow between two parallel disks for three different nanoparticle shapes Platelet, Cylinder, and Brick at varying values of the parameter $A = 2$, 4, and 6. The curves represent the dimensionless temperature $\theta(\eta)$ as a function of the similarity variable η, highlighting how the parameter A influences the thermal behavior of the fluid. As A increases, the temperature profiles exhibit more pronounced curvature, indicating enhanced heat transfer due to stronger squeezing effects. The Platelet-shaped nanoparticles (cyan line) show the most significant deviation in temperature compared to Cylinder (red dashed line) and Brick (magenta dotted line) shapes, reflecting their larger surface area-to-volume ratio and stronger interaction with the base fluid. The convergence of all curves near $\eta = 1$ suggests boundary layer behavior, where the temperature approaches zero at the upper disk. This analysis underscores the critical role of both nanoparticle geometry and the parameter A in controlling the thermal characteristics of nanofluids under squeezed conditions.

Figure 8 illustrates the temperature profiles $\theta(\eta)$ of a magneto-nanofluid flow between two parallel disks for three different nanoparticle shapes Platelet, Cylinder, and Brick at varying values of the parameter $\delta = 0.3$, 0.5, and 0.7. The curves represent the dimensionless temperature $\theta(\eta)$ as a function of the similarity variable η, highlighting how the parameter δ influences the thermal behavior of the fluid. As δ increases, the temperature profiles exhibit more pronounced curvature, indicating enhanced heat transfer due to stronger effects of the parameter δ. The Platelet-shaped nanoparticles (cyan line) show the most significant deviation in temperature compared to Cylinder (red dashed line) and Brick (magenta dotted line) shapes, reflecting their larger surface area-to-volume ratio and stronger interaction with the base fluid. The convergence of all curves near $\eta = 1$ suggests boundary layer behavior, where the temperature approaches zero at the upper disk. This analysis underscores the critical role of both nanoparticle geometry and the parameter δ in controlling the thermal characteristics of nanofluids under squeezed conditions.

Figure 9 illustrates the temperature profiles ($\theta(\eta)$) of a magneto-nanofluid flow between two parallel disks for three different nanoparticle shapes Platelet, Cylinder, and Brick at

International Journal of Advances in Engineering and Management (IJAEM)
Volume 7, Issue 07 July 2025, pp: 500-514 www.ijaem.net ISSN: 2395-5252

varying Eckert numbers (Ec = 0.3, 0.5, and 0.7). The curves represent the dimensionless temperature θ(η) as a function of the similarity variable (η), highlighting how the Eckert number influences the thermal behavior of the fluid. As Ec increases, the temperature profiles exhibit more pronounced curvature, indicating enhanced heat transfer due to stronger viscous dissipation effects. The Platelet-shaped nanoparticles (cyan line) show the most significant deviation in temperature compared to Cylinder (red dashed line) and Brick (magenta dotted line) shapes, reflecting their larger surface area-to-volume ratio and stronger interaction with the base fluid. The convergence of all curves near η = 1 suggests boundary layer behavior, where the temperature approaches zero at the upper disk. This analysis underscores the critical role of both nanoparticle geometry and the Eckert number in controlling the thermal characteristics of nanofluids under squeezed conditions.

Figure 10 illustrates the temperature profiles θ(η) of a magneto-nanofluid flow between two parallel disks for three different nanoparticle shapes Platelet, Cylinder, and Brick at varying Hartmann numbers (M = 3, 6, and 9). The curves represent the dimensionless temperature θ(η) as a function of the similarity variable η, highlighting how the magnetic field strength influences the thermal behavior of the fluid. As M increases, the temperature profiles exhibit more pronounced curvature, indicating enhanced heat transfer due to stronger magnetic effects. The Platelet-shaped nanoparticles (cyan line) show the most significant deviation in temperature compared to Cylinder (red dashed line) and Brick (magenta dotted line) shapes, reflecting their larger surface area-to-volume ratio and stronger interaction with the base fluid. The convergence of all curves near η = 1 suggests boundary layer behavior, where the temperature approaches zero at the upper disk. This analysis underscores the critical role of both nanoparticle geometry and the Hartmann number in controlling the thermal characteristics of nanofluids under squeezed conditions

Figure 11 illustrates the temperature profiles θ(η) of a magneto-nanofluid flow between two parallel disks for three different nanoparticle shapes Platelet, Cylinder, and Brick at varying Prandtl numbers (Pr = 3.5, 3.7, and 3.9). The curves represent the dimensionless temperature θ(η) as a function of the similarity variable η, highlighting how the Prandtl number influences the thermal behavior of the fluid. As Pr increases, the temperature profiles exhibit more pronounced curvature, indicating enhanced heat transfer due to stronger viscous dissipation effects. The Platelet-shaped nanoparticles (cyan line) show the most significant deviation in temperature compared to Cylinder (red dashed line) and Brick (magenta dotted line) shapes, reflecting their larger surface area-to-volume ratio and stronger interaction with the base fluid. The convergence of all curves near η = 1 suggests boundary layer behavior, where the temperature approaches zero at the upper disk. This analysis underscores the critical role of both nanoparticle geometry and the Prandtl number in controlling the thermal characteristics of nanofluids under squeezed conditions.

V. CONCLUSION

This research provides a comprehensive analysis of the MHD squeezing flow and heat transfer of nanofluids between parallel disks, emphasizing the influence of nanoparticle shape factors. The Hamilton-Crosser model effectively captures the thermal conductivity variations due to nanoparticle geometry, with Platelet-shaped nanoparticles showing superior heat transfer performance compared to Cylinder and Brick shapes. The HPM-based solutions reveal that increasing the nanoparticle volume fraction (ϕ) enhances both momentum and thermal transport, while the Hartmann number (M) and squeeze number (S) introduce resistive and squeezing effects, respectively, altering velocity and temperature distributions.

Key findings include:

1. Nanoparticle Shape Dependence: Platelet-shaped nanoparticles yield the highest deviations in velocity and temperature profiles, attributed to their larger sphericity and shape factor (m = 5.7).
2. Magnetic Field Effects: Higher Hartmann numbers decelerate the flow due to Lorentz forces but intensify temperature gradients, improving thermal performance.
3. Thermal Enhancements: The Eckert number (Ec) and Prandtl number (Pr) significantly affect viscous dissipation and thermal boundary layers, with higher values leading to elevated temperatures.

The study underscores the potential of tailored nanofluids for advanced thermal management systems. Future work could explore hybrid nanofluids, transient effects, and experimental validation to bridge theoretical insights with practical applications. This research contributes to the growing body of knowledge on nanofluid dynamics, offering valuable guidelines for optimizing heat transfer in industrial and engineerin system.

REFERENCES

[1] Akbar, N. S. (2015).A new thermal conductivity model with shaped factor ferromagnetism nanoparticles study for the blood flow in non-tapered stenosed arteries.IEEE transactions on nanobioscience, 14(7):780–789.

[2] Akbar,N.S.andButt,A.W.(2016). Ferromagneticeffectsforperistalticflowofcu–waternanofluidfordifferentshapesofnanosize particles.Applied Nanoscience, 6:379–385.

[3] Akbar, N. S. and Khan, Z. H. (2016).Effect of variable thermal conductivity and thermal radiation with cnts suspended nanofluid over a stretching sheet with convective slip boundary conditions: Numerical study.Journal of Molecular Liquids, 222:279–286.

[4] Akbar, N. S., Tripathi, D., and Bég, O. A. (2016a).Modeling nanoparticle geometry effects on peristaltic pumping of medical magnetohydrodynamic nanofluids with heat transfer.Journal of Mechanics in Medicine and Biology, 16(06):1650088.

[5] Akbar,N.S.,Tripathi,D.,Khan,Z.H.,andBég,O .A.(2016b). Anumericalstudyofmagnetohydrodynamictra nsportofnanofluids over a vertical stretching sheet with exponential temperature-dependent viscosity and buoyancy effects.Chemical Physics Letters, 661:20–30.

[6] Asadullah, M., Khan, U., Ahmed, N., Mohyud-Din, S. T., et al. (2016).Analytical and numerical investigation of thermal radia- tion effects on flow of viscous incompressible fluid with stretchable convergent/divergent channels.Journal of Molecular Liquids, 224:768–775.

[7] Aybar, H. Ş., Sharifpur, M., Azizian, M. R., Mehrabi, M., and Meyer, J. P. (2015).A review of thermal conductivity models for nanofluids.Heat Transfer Engineering, 36(13):1085–1110.

[8] Azimi,M.andRiazi,R.(2015). Heattransferanalysisofgo-waternanofluidflowbetweentwoparalleldisks. PropulsionandPower Research, 4(1):23–30.

[9] Choi, S. U. and Eastman, J. A. (1995).Enhancing thermal conductivity of fluids with nanoparticles.Technical report, Argonne National Lab.(ANL), Argonne, IL (United States).

[10] Domairry,G.andAziz,A.(2009).Approximate analysisofmhdsqueezeflowbetweentwoparall eldiskswithsuctionorinjection by homotopy perturbation method.Mathematical Problems in Engineering, 2009(1):603916.

[11] Haq, R. U., Noor, N., and Khan, Z. (2016).Numerical simulation of water based magnetite nanoparticles between two parallel disks.Advanced Powder Technology, 27(4):1568–1575.

[12] Hayat,T.,Yousaf,A.,Mustafa,M.,andAsghar, S.(2012).Influenceofheattransferinthesqueezi ngflowbetweenparalleldisks. ChemicalEngineeringCommunications,199(8):1044–1062.

[13] He,J.-H. (1999).Homotopy perturbation technique.Computer methods in applied mechanics and engineering,178(3-4):257–262.

[14] Khan,U.,Ahmed,N.,andMohyud-Din,S.T.(2016a).Soretanddufoureffectsonflo winconvergingganddivergingchannelswith chemical reaction.Aerospace Science and Technology, 49:135–143.

[15] Khan,U.,Ahmed,N.,andMohyud-Din,S.T.(2016b).Thermo-diffusion,diffusion-thermoandchemicalreactioneffectsonmhd flow of viscous fluid in divergent and convergent channels.Chemical Engineering Science, 141:17–27.

[16] Khan, U., Ahmed, N., and Mohyud-Din, S. T. (2018).Analysis of magnetohydrodynamic flow and heat transfer of cu–water nanofluid between parallel plates for different shapes of nanoparticles.Neural Computing and Applications, 29:695–703.

[17] Khan,U.,Ahmed,N.,Mohyud-Din,S.T.,etal.(2016c).Thermo-diffusionanddiffusion-thermoeffectsonflowofsecondgrade fluid between two inclined plane walls.Journal of Molecular Liquids, 224:1074–1082.

[18] Liao,S.-J.(1995).Anapproximatesolutiontechniqueno tdependingonsmallparameters:aspecialexam ple.InternationalJournal of Non-Linear Mechanics, 30(3):371–380.

[19] Liao, S.-J. (1997).Boundary element method for general nonlinear differential operators.Engineering Analysis with Boundary Elements, 20(2):91–99.

[20] Maxwell,J.C.(1873).Atreatiseonelectricityan dmagnetism.1.

[21] Mohyud Din,S.T.,Khan,U.,Ahmed,N.,andHassan,S.M .(2015).Magnetohydrodynamicflowandheattr ansferofnanofluids in stretchable convergent/divergent channels.Applied

Sciences, 5(4):1639–1664.
[22] Mohyud-Din,S.T.,Noor,M.A.,andWaheed,A.(2009).Variationofparametersmethodforsolvingsixth-orderboundaryvalue problems.Communications of the Korean Mathematical Society, 24(4):605–615.
[23] Mustafa,M.,Hayat,T.,andObaidat,S.(2012).Onheatandmasstransferintheunsteadysqueezingflowbetweenparallelplates. Meccanica,47:1581–1589.
[24] Mustapha, R., Abass, F., Enikuomehin, O., Akanbi, M., andSalau, A.(2024).Anumerical analysis ofthe flowand heat transfer characteristicsofeyringpowellfluidwithmixed convectionoverastratifiedsheet:Convectionontheflowandheattransfer. Journal of the Nigerian Mathematical Society, 43(1):59–79.
[25] Mustapha,R.,Akanbi,M.,Abass,F.,Salau,A., Kazeem,M.,Oyeniran,J.,andRaheem,T.(2025). Anumericalsolutionofeyring-powellmhdnanofluidflowwithconvectivesurfaceconditionanddufour-soretimpactpastaverticalplate:Anumericalsolutionof eyring-powell mhd nanofluid flow.Journal of the Nigerian Mathematical Society, 44(2):189–205.
[26] Shahmohamadi, H., Rahmani, R., Rahnejat, H., Garner, C., and Balodimos, N. (2017).Thermohydrodynamics of lubricant flow with carbon nanoparticles in tribological contacts.Tribology International, 113:50–57.
[27] Shahmohamadi, H. and Rashidi, M. M. (2016).Vim solution of squeezing mhd nanofluid flow in a rotating channel with lower stretching porous surface.Advanced Powder Technology, 27(1):171–178.
[28] Sheikholeslami,M.,Azimi,M.,andGanji,D.D. (2015).Applicationofdifferentialtransformationmethodfornanofluidflowina semi-permeablechannelconsideringmagneticfieldeffect.InternationalJournalforComputational MethodsinEngineeringScience and Mechanics, 16(4):246–255.
[29] Sheikholeslami, M., Ganji, D., andAshorynejad, H.(2013).Investigationofsqueezingunsteadynanofluidflowusingadm.Powder Technology, 239:259–265.
[30] Usman,M.,Nazir,A.,Naheed,Z.,andMohyud-Din,S.T.(2013).Adomian'sdecompositionmethodtosqueezingflowandheat transfer between two parallel disks with velocity slip and temperature jump.Diab. Metab, 1:37–44.
[31] Wazwaz,A.-M.(2006). Themodifieddecompositionmethodforanalyticreatmentofdifferentialequations. Appliedmathematics and computation, 173(1):165–176.
[32] Wikipediacontributors(2025).Squeezeflow — Wikipedia,thefreeencyclopedia.[Online;accessed13-June-2025].